UC San Diego
UC San Diego Electronic Theses and Dissertations

Title
Inter-node Distance Estimation for Subsurface Drifting Hydrophones Using Ambient Acoustic Noise

Permalink
https://escholarship.org/uc/item/1xd4v20k

Author
Yeakle, Riley

Publication Date
2016

Peer reviewed|Thesis/dissertation

UNIVERSITY OF CALIFORNIA, SAN DIEGO

Inter-node Distance Estimation for Subsurface Drifting Hydrophones Using Ambient Acoustic Noise

A Thesis submitted in partial satisfaction of the
requirements for the degree
Master of Science

in

Electrical and Computer Engineering - Intelligent Systems, Robotics, and Control

by

Riley Yeakle

Committee in charge:

> Professor Ryan Kastner, Chair
> Professor William Hodgkiss
> Professor Truong Nguyen

2016

The Thesis of Riley Yeakle is approved, and it is acceptable in quality and form for publication on microfilm and electronically:

_____

_____

_____

Chair

University of California, San Diego

2016

DEDICATION

To my family, and everyone who has supported me on my educational

journey.

EPIGRAPH

The purpose of computing is insight, not numbers.

—Richard Hamming

TABLE OF CONTENTS

ACKNOWLEDGEMENTS

First off, I'd like to thank the Kastner Research Group. It's been an honor working with this group for the past two years.

Next, I'd like to thank Prof. Bill Hodgkiss, whose expertise got me pointed in the right direction on solving the problems presented in this work.

I'd especially like to thank my advisors Ryan Kastner and Curt Schurgers, and lab partner Perry Naughton for their mentorship and collaboration. I am proud to have them as co-authors on a submission to IEEE OCEANS 2016 which contains elements of this work.

Finally, I'd like to give a special thanks to my long time mentor Ryan Kastner. Ryan helped spark my interest in engineering and research before I even started my undergraduate degree and has helped me pursue those interests ever since.

ABSTRACT OF THE THESIS

Inter-node Distance Estimation for Subsurface Drifting Hydrophones Using Ambient Acoustic Noise

by

Riley Yeakle

Master of Science in Electrical and Computer Engineering - Intelligent Systems, Robotics, and Control

University of California, San Diego, 2016

Professor Ryan Kastner, Chair

As the number of units in underwater sensor arrays grow, low-cost localization becomes increasingly important to maintain network scalability. Methods using ambient ocean noise are promising solutions because they do not require external infrastructure, nor expensive on-board sensors. Here we extend past work in stationary array element localization from correlations of ambient noise to a mobile sensor array. After obtaining inter-node distance estimates using ambient noise correlations, these distances can be used to determine a relative localization of an array of mobile

underwater sensor platforms without introducing any external infrastructure or on-board localization sensors.

In this work we explore the effects of receiver mobility on inter-node distance estimation via correlations of ambient acoustic noise. Through analysis and simulation, we develop an exact solution along with a more tractable approximation to the peak amplitude of the time-domain Green's function between the two mobile receivers, which provides an estimate of their spatial separation. Here we demonstrate that the mobile noise correlation amplitude at the average time delay between the receivers can be modeled with the wideband ambiguity function of a single sound source. We then use this approximation to discuss selection of design parameters and their effects on the noise correlation function.

This work acts as a piece in the larger problem of infrastructure-free localization for mobile underwater sensor networks. Combining a relative localization from this method with the absolute positions of several units could provide an absolute localization of an entire array, without the need for external infrastructure.

Chapter 1

Introduction

In this thesis I explore the problem of estimating distances between pairs of subsurface drifting hydrophones through correlations of ambient acoustic noise. This chapter introduces the motivating examples for this work, presents approaches to solving these problems, and outlines the contributions of this thesis.

1.1   The Motivating Problem

Understanding the planet's oceans is key because of the critical role they play in our planet's health. Ocean monitoring via sensor networks can be challenging because of the difficulty of communicating with underwater sensor platforms. Beneath the surface, devices no longer have access to radio communications, including GPS which makes localization quite challenging.

The Scripps Institution of Oceanography Autonomous Underwater Explorers (AUEs) are a swarm of drifting underwater sensor platforms which collectively sample a large area densely in both space and time [1] [2]. After deployment, the AUEs

adjust their buoyancy to follow a given depth profile, then drift with the currents while recording temperature and acoustics. The challenge after retrieving the AUEs at the end of their deployment is finding the path they took underwater. Past work uses high frequency pings from surface buoys in the recorded audio to map the paths of each individual drifter through the course of the deployment [3]. These surface pingers are analogous to the satellites used in terrestrial GPS localization systems.

While the pingers provide a good localization solution for the mean time, ideally we could localize the AUEs without introducing extra infrastructure. The pinger based localization system is non-ideal because it limits the system's scalability. Apart from the extra equipment cost, surface currents and subsurface currents often differ, so the pingers can drift away from the AUE swarm over time, limiting the duration of our deployments.

Though the ultimate goal is to globally localize the AUE swarm, this thesis will focus on the sub-problem of relative localization. Specifically we will address the challenge of estimating inter-node distances between receiver pairs. From past work in sensor network localization, we know that a set of pairwise distance estimates for all the nodes in our network is sufficient to come up with a relative localization for the network [4] [9]. This can then turn into a global localization solution if we know the absolute positions of a few 'anchor units'. Finding inter-node distances at different times during the deployment using ambient sounds is a good place to start since we have some promising results from geophysics to build upon.

1.2   Solution Approaches

Our first approach in finding these pairwise distances is to directly apply past work which shows that long term correlations of ambient noise recorded at two nearby hydrophones can estimate the time-domain Green's function (analogous to the impulse response in linear systems theory) between the two receivers [5]. Here we will build on past work by extending this theory to the mobile receiver case. This will give us a handle on what sorts of mobility conditions we can estimate pairwise distances between drifters under ideal sound field conditions.

After finding the effects of receiver velocity on our noise correlation function we can find how velocity fits in with other design parameters in the noise correlation process. For the stationary receiver case, we know from past work [6] that the correlation window length and bandwidth both reduce the noise level seen in the time-domain Green's function. Thus in the stationary case, a good strategy would be to use a long time window and large bandwidth. However, when our receivers are mobile, longer time windows are not necessarily better. Understanding how receiver velocity relates to the noise correlation function will allow us to relate the parameters center frequency (f_c), bandwidth (B), correlation window (T), and velocity into a design space which will predict the viability of noise correlation as a means of distance estimation in a given environment.

1.3   Outline of Contributions

This thesis will:

- Explore how receiver velocity affects the noise correlation function and thus our

ability to recover pairwise distances via ambient noise correlation.

- Present an approximation to the amplitude of the noise correlation function at the time lag corresponding to the distance between the receivers using the wideband ambiguity function for a single bandpass source on the axis passing through the receivers.

- Analyze how these velocity effects will impact the choice of correlation parameters like window length, center frequency, and bandwidth.

- Demonstrate how the results presented can be used to find the maximum tolerable inter-node velocity for noise correlation function estimation to achieve a given performance.

Chapter 2

Background and Related Work

This chapter introduces the past research that this thesis builds upon, including ambient noise sources in the ocean, the noise correlation function as an approximation to the time-domain Green's function between receivers, and the wideband ambiguity function, which describes the effects of receiver velocity on cross correlation of a single source.

2.1 Ambient Noise in the Ocean

In this work, we are interested in inferring localization information on our drifting receivers using natural sound sources in the ocean. Depending on the frequency of interest, the ambient acoustic noise in the ocean comes from a variety of sources [7]. Seismic activity, shipping noise, surface agitation, and even bubbles all generate noise in the ocean [7]. In particular, we will be interested in noise in the 100 to 1000 Hz frequency range, a band typically dominated by shipping noise and surface agitation [7]. While shipping noise can be used in the stationary receiver case to infer distance

information between receivers via noise correlation [8], it requires long correlation windows to overcome the strong directionality of the ship's noise. Thus for this work, we are primarily concerned with noise from biological sources and surface agitations.

2.2 The Time Domain Green's Function

The key result this thesis builds on is the emergence of an estimate of the time-domain Green's function from correlations of ambient acoustic noise. The time-domain Green's function describes the propagation of a wave from one point in space to another and is analogous to the impulse response used in linear systems theory. In the context of sensor networks, the time-domain Green's function (now referred to as TDGF) between two receivers tells us how a source will propagate from one receiver to the other and by knowing the direct path arrival and the speed of sound in our medium, we can then estimate the distance between those two receivers.

The noise correlation function itself actually converges to an estimate of the time-domain Green's function, with the actual TDGF equivalent to the derivative of the noise correlation function. In practice, the noise correlation function is close enough to the actual TDGF that the approximation is worth the computational ease of working with the noise correlation function rather than its derivative. Here I give an intuitive explanation for the emergence of the TDGF from ambient acoustic noise correlations, however interested readers may refer to [5] and [8] for rigorous derivation as well as field experiments demonstrating successful estimation of distances between receiver pairs.

The first insight in developing the theory of ambient noise correlation is that the cross correlation function has a well-defined directivity pattern, meaning *it is*

sensitive to sources originating from certain directions more than others. To see this, consider the following scenario, two receivers r_1 and r_2 separated by a distance R in a 2D plane. Under cross correlation, an source will give us an peak centered at time $\frac{d_{s1} - d_{s2}}{c}$ where d_{si} is the distance from the source to receiver i. As a function of angle of approach θ_0, defined with respect to the axis between our receiver pair, the time delay produced by a single source under cross correlation is given by:

$$\tau_s = \frac{R}{c} \cos(\theta_0) \tag{2.1}$$

Thus, we expect sources near the axis of the receivers ($\theta_0 \approx 0$ and $\theta_0 \approx \pi$) to produce delay estimates closer in time to each other than those near $\theta_0 = \pm\frac{\pi}{2}$. Consequentially, we expect larger correlation peaks to build up near τ corresponding to $\theta_0 \approx 0$ or π than anywhere else. Specifically, this τ is $\pm\frac{R}{c}$ gives the time of flight from one receiver to the other. As demonstrated in [8], the relative proportion of sources contributing to the correlation peak at $\tau = \pm\frac{R}{c}$ can be modeled using the directivity of the correlation function. Using this, the authors in [8] show that the ratio of 'coherent' sources (sources contributing to a correlation peak at $\tau = \pm\frac{R}{c}$), versus 'incoherent' sources (those contributing to correlation peaks elsewhere) can be expressed as:

$$Ratio(\theta_0) = \sqrt{\frac{2\pi f_c}{c}} R \left(1 + \frac{1}{12} \left(\frac{B}{f_c} \right)^2 \right)^{\frac{1}{4}} \sin(\theta_0) \tag{2.2}$$

where θ_0 is the angle of approach. In an isotropic sound field (meaning uniformly distributed source locations), the number of coherent sources is far greater than any θ_0 corresponding to a different time difference of arrival. Thus by correlating over

long time windows the noise correlation function produces roughly symmetric peaks at $\tau = \pm\frac{R}{c}$.

Borrowing vocabulary from [8] and [9], we use the term 'endfire' to refer to the region around $\theta \in \{0, \pi\}$ for which sound sources make a significant contribution to the correlation peak at $\tau = \pm\frac{R}{c}$. We can define this region more specifically using the directivity of the cross correlation function between our receivers and choosing the angle $\theta_{endfire}$ to be the effective beamwidth of the beam centered on $\theta = 0$ or equivalently $\theta = \pi$.

An important factor in the success of this technique is the actual distribution of the sounds in our environment. Though proven to work in common ocean ambient sound environments, like surface noise [8], this technique is sensitive to dominant sound sources. As shown in [8], dominant sources like shipping noise can bias the peak locations of the noise correlation function. This is especially relevant in the mobile receiver case examined in this thesis in which we cannot use long correlation windows to compensate for strong sources in the environment.

To get the cleanest correlation results, past work (and this work) implements the following preprocessing pipeline shown in Figure 2.1 to compute the noise correlation function. After preprocessing, we compute the noise correlation function using:

$$C_{y_1, y_2}(\tau) = \frac{1}{T} \int_{-T/2}^{T/2} y_1(t) y_2(t - \tau) dt \tag{2.3}$$

$$NCF_{y_1, y_2}(\tau) = \frac{C_{y_1, y_2}(\tau)}{\left(\frac{1}{T} \int_{-T/2}^{T/2} y_1^2(t) dt\right)^{\frac{1}{2}} \left(\frac{1}{T} \int_{-T/2}^{T/2} y_2^2(t - \tau) dt\right)^{\frac{1}{2}}} \tag{2.4}$$

In preprocessing, the bandpass step gives us control over what sorts of ambient
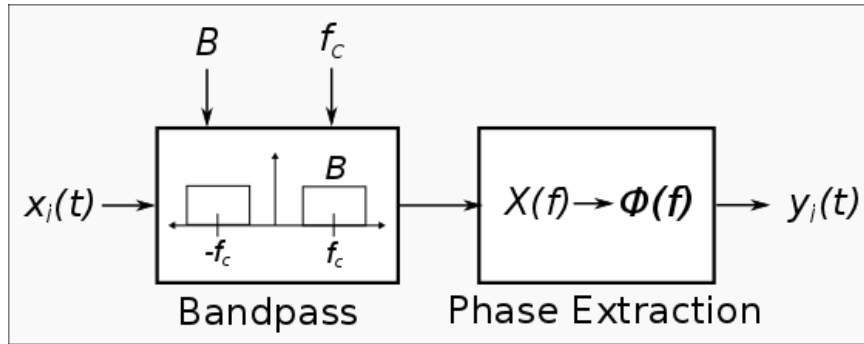
Figure 2.1: Preprocessing pipeline used to compute the noise correlation function. The bandpass step allows us to focus on a specific noise frequency band, and the whitening step prevents the correlation from being biased by dominant frequency components.

sounds we look at, and we'll later see has an effect on our system's resilience to receiver velocity. The whitening step in which we extract the phase of the received signal ensures that our correlation process does not get dominated by any strong frequencies. Since we're only interested in the location of our peak, not so much its amplitude, we don't lose information necessary to estimate the distance between receivers by doing this.

2.3   The Wideband Ambiguity Function

In finding how receiver velocity will affect the noise correlation function, it's key to understand how receiver velocity affects the correlation between two receivers of a single source. Because of its strong applicability to detection of moving targets with reflected radar pulses, this is a well studied problem.

For a single source, this problem is modeled by the wideband ambiguity function, originally developed for studying radar responses to high velocity targets using broad spectrum radar pulses [10]. The ambiguity function describes the matched

filter response of a delayed and Doppler mismatched pulse. In computing the noise correlation function over a single source, we are essentially running a matched filter across our receivers and thus the wideband ambiguity function describes how our correlation will behave with receiver velocity and delay errors. Since we are interested in wideband signals in this work, Woodward's original ambiguity function [11], which uses a constant frequency shift to approximate Doppler mismatch is not suitable. As shown in [10] for a single source s, the wideband ambiguity function for cross correlation can be written as:

$$A(\tau, \beta) = \int s(t)s^*(\beta(t+\tau))dt \tag{2.5}$$

In particular we will be interested in the normalized version of this function for a broadband, flat spectrum, Gaussian signal. Normalized in this case meaning we want to know the correlation coefficient between the original signal and the Doppler shifted and delayed signal. In [12] the authors compute the normalized ambiguity function for just that signal and find the following:

$$\rho(\gamma = 0, \dot{\mu}) = \frac{1}{2b} \left[Si((a+1)b) - Si((a-1)b) \right] \tag{2.6}$$

with:

$$Si(x) = \int_0^x \frac{\sin x}{x} \, dx$$

and $a = \frac{2}{f_c}$, and $b = \frac{\pi}{2}(B\dot{\mu}T)$, where f_c denotes the center frequency of our signal, B denotes its one-sided bandwidth, and T denotes the length of our correlation window, γ indicates the delay error, and $\dot{\mu}$ denotes the rate of change for the time delay between our two receivers. For a single mobile receiver, $\dot{\mu} = \frac{v_{rel}}{c}$ and for two mobile receivers it

is given as $\frac{1+\frac{v_2}{c}\cos(\theta_2)}{1+\frac{v_1}{c}\cos(\theta_1)} - 1.$
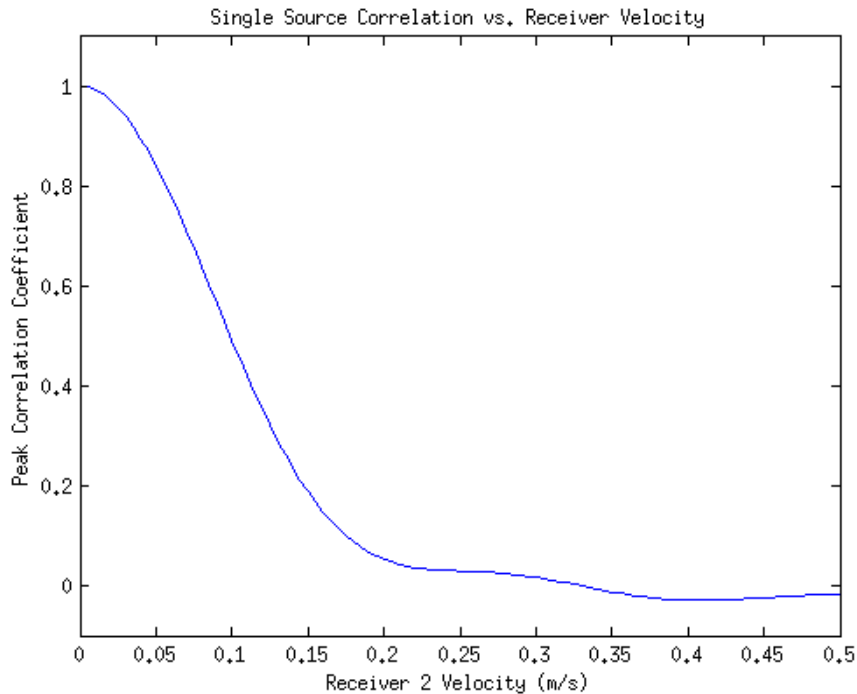
Figure 2.2: Example of a zero time delay error cut of the normalized ambiguity function for a broadband, flat spectrum, Gaussian pulse.

This function represents the zero delay error cut of the ambiguity function of the matched filter over two receivers, which describes the correlation peak as a function at time delay $\tau = D$ and relative Doppler shift across each receiver $\dot{\mu}$. An interesting feature of the ambiguity function is that for some signals, it shows a phenomenon called 'range-Doppler coupling' in which the maximum value of the ambiguity function for a given velocity is *not* at the zero delay error time. In this work, we will focus on the zero time delay cut of the ambiguity function, however in future developments, this is something to keep in mind.

In Chapter 3 we will use the wideband ambiguity function to develop a theory on how receiver velocity will affect the emergence of the time-domain Green's function from the correlations of many ambient noise sources.

2.4 Noise Correlation SNR

After finding the relationship between receiver velocity and noise correlation value at $\tau = \pm\frac{R}{c}$, we'll be interested in finding how mobility affects the noise correlation signal to noise ratio. Combining past work on the signal to noise ratio of the noise correlation function with mobility loss we'll be able to address the issue of choosing a correlation time window that is both long enough for our distance estimate to emerge, but short enough to not be destroyed by receiver mobility.

In [9], the authors study the signal to noise ratio of the noise correlation function as a distance estimator. The signal to noise ratio (SNR) for this this problem is defined as:

$$SNR = \frac{1}{2}\left(\frac{NCF(\tau^+)}{std(NCF(\tau))_{\tau>10\tau^+}} + \frac{NCF(\tau^-)}{std(NCF(\tau))_{\tau<10\tau^-}}\right) \tag{2.7}$$

The authors then show this signal to noise ratio is proportional to the following:

$$SNR \propto \left(\frac{\sqrt{BT}}{\sqrt{k_c R}}\right)e^{-\alpha R} \tag{2.8}$$

where k_c is the wavenumber corresponding to our center frequency f_c, and α measures our bottom loss absorption.

In this work we are interested in just the terms that relate to the correlation parameters we have some control over, B, f_c, and T. Thus, we will focus on:

$$SNR \propto \left(\frac{\sqrt{BT}}{\sqrt{f_c}}\right) \tag{2.9}$$

when relating the choice of correlation parameters to SNR under receiver mobility.

Looking at 4.1 we can see that the SNR for stationary receivers is increasing with the time-bandwidth product and decreasing with increasing center frequency, indicating that a large bandwidth and time window, with a low center frequency will yield the best results.

Chapter 3

Velocity Effects on the Noise Correlation Function

This chapters develops theory on how the noise correlation function will degrade as a function of receiver velocity then presents simulation results which test those ideas. We begin by developing an exact solution of the noise correlation function under receiver velocity where we find the normalized ambiguity function for our individual sources embedded in some expectations over the actual distribution of sources. Since this provides little insight into how receiver mobility affects the noise correlation function, we then develop an approximation which treats sources in the endfire region as a single 'virtual source'. This approximation describes the effects of velocity on the noise correlation function in a much simpler context, yielding insight into how we expect the noise correlation function to behave with mobile receivers.
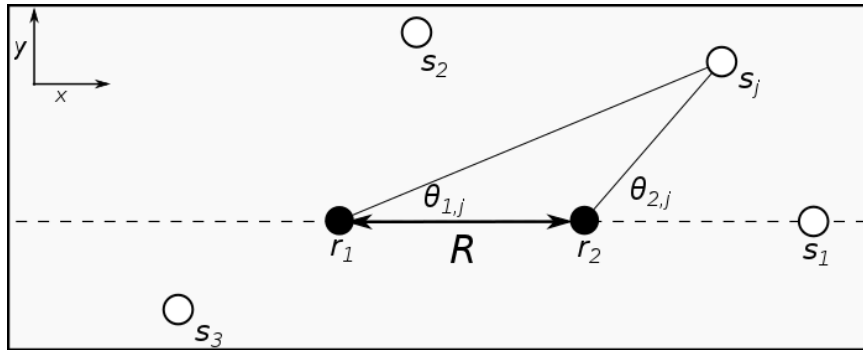
Figure 3.1: Example of receiver and source setup in a 2D plane. Sources s_1 to s_j are distributed around the receiver pair and represent active sources at this instant in time. Receivers r_1 and r_2 are separated by a distance R and each have velocity v_i along the axis passing through the pair.

3.1 Problem Formulation

We make the following assumptions to develop our theory on the effects of receiver mobility during noise correlation:

- Our sources are stationary in space

- Our sources are transient in time

- Our sources are generated from uncorrelated Gaussian processes with mean 0 and variance σ_s^2

- Our sources have a flat spectrum extending beyond the bandwidth over which we correlate

- All sources propagate in a single direct path from source to receiver and undergo attenuation due to spherical spreading proportional to $\frac{1}{r}$ where r is the distance traveled from the source's origin

- In correlation preprocessing, we use $f_{min} \geq 100Hz$

- There are a large number of sound events over our correlation time window

- Our receiver velocity is significantly less than the speed of sound in the medium

- Receiver velocity is taken with respect to the axis through the receivers

These assumptions form the simplest case that is still interesting for describing the effect of receiver motion on the noise correlation function. Sources that are stationary in space and transient in time is reasonable given our previous discussion of our noise sources of interest. Our assumption of correlation bandwidth smaller than the noise bandwidth is reasonable so long as we choose our bandwidth and center frequency in a manner consistent with the actual spectrum of ambient ocean noise. Given our practical application of the AUEs, our assumption of small relative velocity is very reasonable since they are all carried by the subsurface currents. For example, in a previous deployment of the AUEs we found that the units tend to move less than $0.2m/s$ with respect to each other over 12 second intervals as shown in Figure 3.2. The constraint of $f_{min} \geq 100Hz$ ensures that our correlation directivity intuition holds since low frequencies exhibit much less directivity than higher frequencies.

We choose to take the receiver velocity along the axis because in a relatively uniform spatial distribution of short sound events, the relevant velocity term is how much the receivers move with respect to each other since the sound field looks the same in all directions. In a more directional sound field, the rotation of the receivers would be important because it would affect the distribution of sources in the endfire regions over time. However, strongly directional sound fields tend to distort the emergence of the time-domain Green's function from correlations of ambient noise, so this method is unsuitable for those environments.
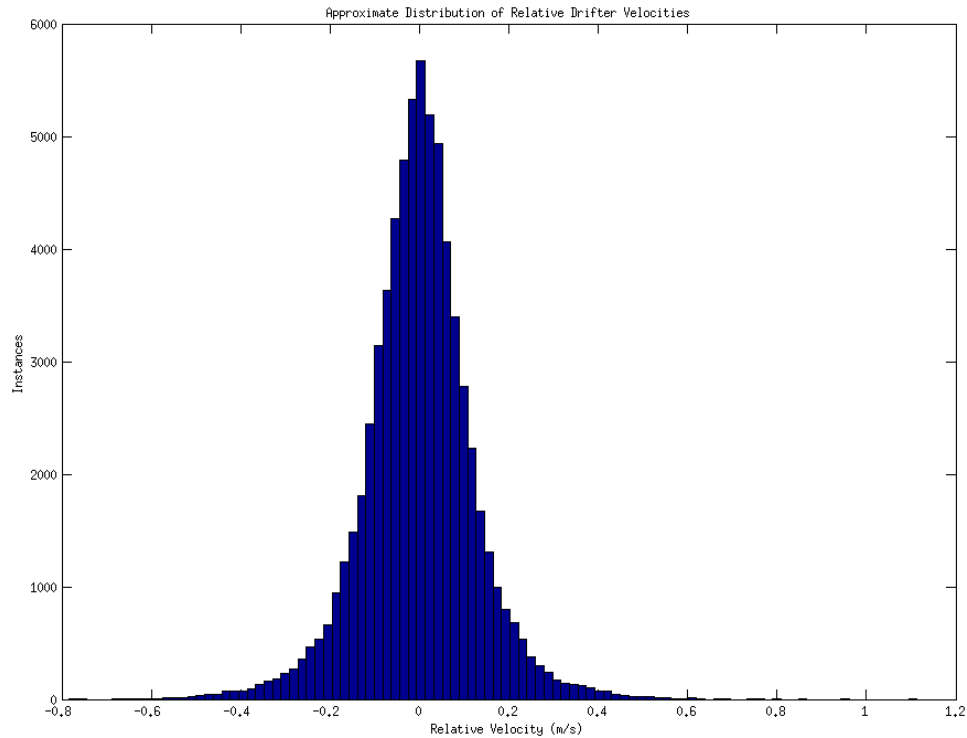
Figure 3.2: Histogram of relative velocities between AUEs from a past deployment demonstrates that our units tend to have low relative velocity with respect to each other.

The weakest assumption here for practical environments is that of direct path propagation with spherical spreading loss. The underwater acoustic channel is very complex and highly variant over different environments. However, for these experiments our goal is to build insight into the behavior of the noise correlation function in the presence of receiver mobility. These more complex models may be appropriate if the fundamental theory we develop here fails to capture the general behavior of the noise correlation function elsewhere.

3.2 Correlation Directivity and Velocity Effects on a Single Source

In this section we explore how receiver velocity and correlation directivity affect the relative importance of sources approaching from different angles θ_0. Without receiver motion, sources close to $\theta_0 \in \{0, \pi\}$ have the biggest contribution to the noise correlation function at $\tau = \pm \frac{R}{c}$. However when the receivers are moving, the receivers have the highest relative velocity to sources on the axis and thus these sources will experience the most velocity loss. Our goal here is to distil these competing effects in order to choose an appropriate model for sources in the endfire region.
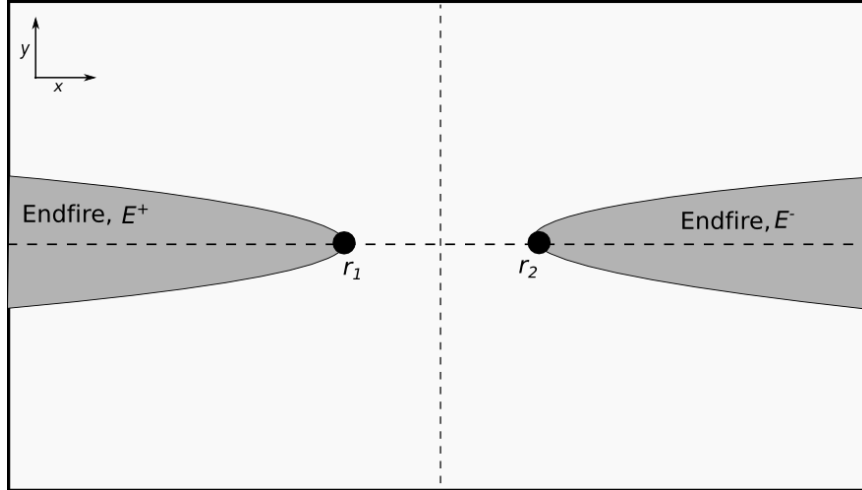
Figure 3.3: Receiver geometry showing endfire regions. Sources in these beams contribute to correlation peaks at $\tau = \pm \frac{R}{c}$ under cross correlation.

Noting that the relative velocity of our receivers with respect to a source off the axis is less than the axis source case, we see that when our receivers are moving, there are two competing effects driving the correlation amplitude of sources coming from direction θ_0. While sources near the axis of the receivers experience the most velocity distortion, they also make the biggest contributions to the noise correlation function.

One way to think about the effects of different sources on the noise correlation is to assign a weight to each source based on its angle of approach to the receiver pair. This weight can be broken into two components, the correlation directivity effect, and the velocity distortion effect.

The amplitude of the noise correlation function is proportional to the number of sources making significant contributions to each specific time lag. From [8] we know that the ratio of the area enclosed by the endfire beam to a non-endfire direction θ_0 is

$$Ratio(\theta_0) = \sqrt{\frac{2\pi f_c}{c}} R \left(1 + \frac{1}{12} \left(\frac{B}{f_c} \right)^2 \right)^{\frac{1}{4}} \sin(\theta_0) \qquad (3.1)$$

This ratio comes from formulating approximations for the directivity of the correlation function for endfire and non-endfire beams, using those to compute beamwidth angles for on and off endfire angles, then finding the ratio of the two terms. Note that this relationship holds only for θ_0 off the endfire line. We can also think of this ratio as the correlation directivity weight of a source in the endfire compared to another beam.

With one moving receiver we can write the relative velocity of the receiver with respect to a source s approaching from an angle θ_0 as $v_i \cos(\theta_i)$ we can then express the overall velocity weight for a source approaching from various angles for a fixed receiver velocity using the normalized wideband ambiguity function as:

$$\rho_s \left(0, \frac{v_i}{c} \cos(\theta_0) \right) \qquad (3.2)$$

Let $V(\theta_0)$ be the ratio of the velocity loss for a source on the endfire to the velocity loss of a source in the far field approaching from the angle θ_0. This captures

the relative weighting of a source due to receiver velocity, which we can write this as:

$$V(\theta_0) = \frac{\rho\left(0, \frac{v_i}{c}\right)}{\rho\left(0, \frac{v_i}{c}\cos(\theta_0)\right)} \tag{3.3}$$

Figure 3.4 shows an example of this dropoff for receiver velocities of $v_1 = 0$ and $v_2 = 0.1$.
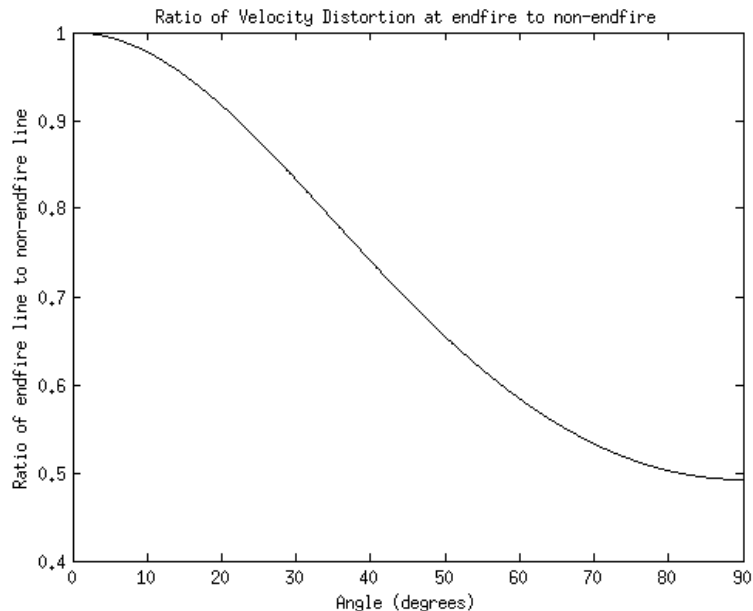
Figure 3.4: Ratio of ambiguity function for a source in the endfire at zero delay error to that of a source approaching from a different angle. This shows that in the endfire region the velocity effect is small, but increases as we move farther off axis.

Combining equations 3.1 and 3.3 to form a total weight for a given source in the endfire compared to a source in another beam as $Ratio(\theta_0)V(\theta_0)$ we can see that for small θ_0 in our endfire beam, the velocity weighting term stays near one. Thus for sources in the endfire region, the correlation directivity dominates the overall weight for a given source, while in the $\theta = \pm\frac{\pi}{2}$ region, the reduced distortion from the smaller source-receiver relative velocity has a noticeable effect on the contribution of

the source to the correlation function.

3.3 Exact Solution

Here we build on the previous section to relate the normalized ambiguity function for a single source $\rho(\gamma = 0, \dot{\mu})$ to the noise correlation function at time $\tau = \pm\frac{R}{c}$ in the presence of constant receiver velocity.

In a field of j sound sources, we can write the signal received at receiver i as:

$$x_i(t) = \sum_{j=1}^{N} \alpha_{i,j} s_j((\beta_{i,j}(t + \mu_{i,j}) + D_j) \tag{3.4}$$

where $\alpha_{i,j}$ is the attenuation between source j and receiver i, $\beta_{i,j}$ is the time scaling between source i and receiver j (with $\beta_{i,j} = (1 + \frac{v_i}{c}\cos(\theta_{i,j}))$, $\mu_{i,j}$ is the time delay for the source traveling to the receiver at the start of correlation, and D_j is the start time of source j.

Next, we define the following:

$$\hat{\sigma}_y = \sqrt{\int_{-\frac{T}{2}}^{\frac{T}{2}} y^2(t)dt} \tag{3.5}$$

as the square root of the energy of a signal $y(t)$.

Next, we have the correlation coefficient $\rho_{y_1,y_2}(\tau)$ given by:

$$\rho_{y_1,y_2}(\tau) = \frac{1}{\hat{\sigma}_{y_1}\hat{\sigma}_{y_2}} \left(\frac{1}{T} \int_{-\frac{T}{2}}^{\frac{T}{2}} y_1(t)y_2(t - \tau)dt \right) \tag{3.6}$$

Finally, let $y'(t)$ be the ideal bandpass filtered version of $y(t)$, as performed in the noise correlation pre-processing step before whitening. We can then relate the

noise correlation function to the velocity correlation coefficients for each individual source in our field as follows:

$$NCF_{x_1,x_2}(\tau, t, v_1, v_2) = \rho_{x_1',x_2'}(\tau) \tag{3.7}$$

$$= \frac{1}{\hat{\sigma}_{x_1'}\hat{\sigma}_{x_2'}} \frac{1}{T} \int_{-\frac{T}{2}}^{\frac{T}{2}} x_1'(t)x_2'(t-\tau)dt \tag{3.8}$$

Then, since we assume uncorrelated sources, the cross terms in the product $x_1'(t)x_2'(t-\tau)$ cancel and we are left with:

$$\frac{1}{\hat{\sigma}_{x_1'}\hat{\sigma}_{x_2'}} \sum_{j=1}^{N} \alpha_{1,j}\alpha_{2,j} \frac{1}{T} \int_{-\frac{T}{2}}^{\frac{T}{2}} s_{1,j}'(t)s_{2,j}'(t-\tau)dt \tag{3.9}$$

Since $s_{1,j}'$ and $s_{2,j}'$ are related as time scaled and shifted versions of each other, we can replace the integral with their normalized ambiguity function to obtain:

$$\frac{1}{\hat{\sigma}_{x_1'}\hat{\sigma}_{x_2'}} \sum_{j=1}^{N} \alpha_{1,j}\alpha_{2,j}\hat{\sigma}_{s_{1,j}'}\hat{\sigma}_{s_{2,j}'}\rho_{s_{1,j}',s_{2,j}'}(\tau, \dot{\mu}_j) \tag{3.10}$$

Next, we break this down a bit further to gain insight as to how this varies from the noise correlation function for stationary receivers. The key is in understanding the $\hat{\sigma}_{x_i'}$ term. Using our given equations for x_i, this reduces to:

$$\hat{\sigma}_{x_i'} = \sqrt{\sum_{j=1}^{N} \alpha_{i,j}^2 \sigma_{s_{i,j}'}^2} \tag{3.11}$$

$$= \sqrt{NE\left[\alpha_{i,j}^2 2 \int_{f_{min}}^{f_{max}} \frac{1}{|\beta_{i,j}|^2} \left|S_j\left(\frac{f}{\beta_{i,j}}\right)\right|^2 df\right]} \tag{3.12}$$

with $S_j(f)$ as the Fourier transform of $s_j(t)$. Applying a change of variables of $g = \frac{f}{\beta_{i,j}}$ and assuming a constant magnitude of $S_j(f)$ for $\frac{f_{min}}{\beta_{i,j}} \leq f \leq \frac{f_{max}}{\beta_{i,j}}$ we obtain:

$$\hat{\sigma}_{x_i'} = \sqrt{N\hat{\sigma}_{s_j}^2 E\left[\frac{\alpha_{i,j}^2}{\beta_{i,j}^2}\right]} \tag{3.13}$$

$$= \sigma_{s'}\sqrt{NE\left[\frac{\alpha_{i,j}^2}{\beta_{i,j}^2}\right]} \tag{3.14}$$

We then apply this back to 3.10 to obtain:

$$NCF_{x_1,x_2}(\tau, t, v_1, v_2) = \frac{\sum_{j=1}^{N} \alpha_{1,j}\alpha_{2,j}\hat{\sigma}_{s_{1,j}'}\hat{\sigma}_{s_{2,j}'}\rho_{s_{1,j}',s_{2,j}'}(\tau, \dot{\mu}_j)}{N\sigma_{s'}^2\sqrt{E\left[\frac{\alpha_{1,j}^2}{\beta_{1,j}^2}\right] E\left[\frac{\alpha_{2,j}^2}{\beta_{2,j}^2}\right]}} \tag{3.15}$$

Noting that the numerator converges to its expected value for large N as well, we finally obtain:

$$NCF_{x_1,x_2}(\tau, t, v_1, v_2) = \frac{E\left[\alpha_{1,j}\alpha_{2,j}\hat{\sigma}_{s'_{1,j}}\hat{\sigma}_{s'_{2,j}}\rho_{s'_{1,j},s'_{2,j}}(\tau, \dot{\mu}_j)\right]}{\sigma_{s'}^2\sqrt{E\left[\frac{\alpha_{1,j}^2}{\beta_{1,j}^2}\right]E\left[\frac{\alpha_{2,j}^2}{\beta_{2,j}^2}\right]}} \tag{3.16}$$

$$= \frac{E\left[\frac{\alpha_{1,j}}{\beta_{1,j}}\frac{\alpha_{2,j}}{\beta_{2,j}}\rho_{s'_{1,j},s'_{2,j}}(\tau, \dot{\mu}_j)\right]}{\sqrt{E\left[\frac{\alpha_{1,j}^2}{\beta_{1,j}^2}\right]E\left[\frac{\alpha_{2,j}^2}{\beta_{2,j}^2}\right]}} \tag{3.17}$$

3.4   Developing a Useful Approximation

While Equation 3.16 gives us an exact expression for the noise correlation function between two moving receivers in a sound field with a known distribution, it is not particularly insightful in this form. Here we develop an approximation relating the noise correlation function amplitude at the average receiver separation over T as a function of velocity to the correlation coefficient of a single source across the two receivers. Approximating the noise correlation function under receiver velocity in this way will allow us to use our the matched filter ambiguity function for a single broadband source to describe the behavior of the noise correlation function for mobile receivers.

3.4.1   Behavior of Endfire Sources

We first note that only sources inside the endfire beam will make significant contributions to the noise correlation function. Sources outside this beam (approaching from an angle greater than $\theta_{endfire}$) do not make a meaningful contribution to the noise correlation peak at $\tau = +\frac{R}{c}$ (which we will refer to as τ^+). For mobile receivers, this peak appears centered on the average time difference from one receiver to the
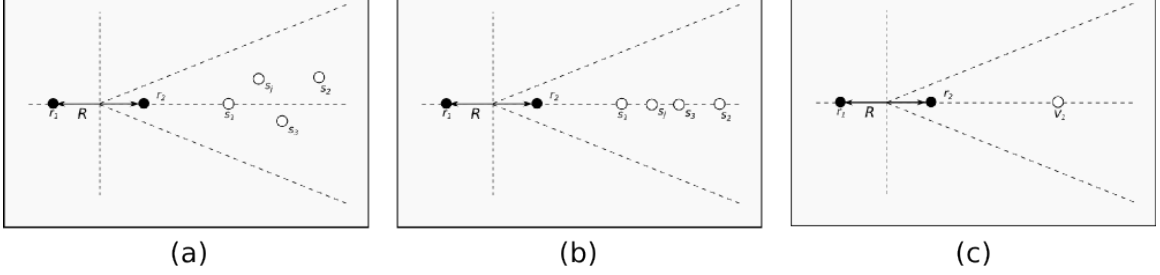
Figure 3.5: Virtual source argument in pictures demonstrates how we can represent a set of sources in the endfire region as a single virtual source. (a): We begin with a set of sources in the endfire region (b): Due to the small angle of sources in the endfire region, we can nudge off-axis sources onto the axis through the receivers with approximately the same effect on the receivers. (c): Now that the receiver velocity with respect to all these sources is the same we can replace the sources with a single virtual source with a time series equivalent to the sum of the axis sources. After noise correlation preprocessing, this behaves the same as the collective effect of all the endfire sources.

other over the course of the correlation because the ambiguity function is maximum at that time. Note that the net effect of these sources as heard by receiver i can be written as:

$$x_i(t) = \sum_{j \in E^+} \alpha_{i,j} s_j(\beta_{i,j}(t + D_{i,j})) \tag{3.18}$$

where E^+ denotes the set of sources in the endfire beam corresponding to τ^+.

The key insight in developing our approximation is that these sources in the endfire beam collectively can be approximated with a single source. Recall that $\beta_{i,j} = 1 + \frac{v_i}{c} \cos(\theta_{i,j})$ and that in an endfire beam, $\cos(\theta_{i,j})$ is near 1 for all sources and both receivers. Thus, we can approximate $\beta_{i,j}$ in the endfire region using this small angle approximation for cosine as $\beta_{i,j} \approx 1 + \frac{v_i}{c}$, removing the dependence on θ for the velocity term. Physically, this approximation is equivalent to nudging all endfire sources onto the axis passing through the receivers. This new process behaves like a single source on the axis passing through the receivers since the received signal

$x(t)$ is the same if we replace the set of sources now on the axis with a single source equal to a linear combination of the individual sources on the axis. Since the orginal sources are all Gaussian, this virtual source is as well.

Finally, to demonstrate the applicability of the Gaussian matched filter wideband ambiguity function to the model, we show that after pre-filtering, the virtual source produces a pre-correlation term with flat power spectrum over a given bandwidth. For a single source with receiver motion, in the frequency domain we get the following:

$$S_{i,j}(f) = \left| \frac{1}{\beta_{i,j}} \right| S_j \left(\frac{f}{\beta_{i,j}} \right) e^{-j2\pi f D_{i,j} \beta_{i,j}} \tag{3.19}$$

From 3.19 we can see that the receiver motion either expands or contracts the original source spectrum by a relatively small amount since for low receiver velocity $\beta_{i,j} \approx 1$ since we assume that $\frac{v_i}{c} \ll 1$. By linearity of the Fourier transform, we can then see that the received signal spectrum for a set of sources will be a slightly dilated version of the original spectrum. After bandpassing out our frequencies of interest and whitening via extracting the Fourier transform phase, we're left with spectral properties matching what we would see in the stationary case. Therefore we can approximate the set of sources in the endfire beam during the correlation window as a single virtual source. The mobile noise correlation function for this virtual source is then given by the normalized wideband ambiguity function for a broadband, flat spectrum source. Next, we relate this approximation back to the full field noise correlation function to predict the noise correlation function value at $\tau = \pm \frac{R}{c}$ in the full noise field case.

3.4.2 Relationship to Stationary Noise Correlation Function

Under this virtual source argument, we are approximating the net effect of all our endfire sources with a single axis source. We now need to show what happens to this function when we include the noise from sound sources outside the endfire beam. Combining this approximation for the sources in our endfire beam with the exact solution presented in equation 3.16 we get:

$$NCF(\tau^+, v_1, v_2) \approx \frac{\sum_{j \in E^+} \left[\frac{\alpha_{1,j}}{\beta_{1,j}} \frac{\alpha_{2,j}}{\beta_{2,j}} \right]}{N \sqrt{E \left[\frac{\alpha_{1,j}^2}{\beta_{1,j}^2} \right] E \left[\frac{\alpha_{2,j}^2}{\beta_{2,j}^2} \right]}} \rho(0, \dot{\mu}_{axis}) \tag{3.20}$$

The term in front of the normalized ambiguity function cut $\rho(0, \dot{\mu}_{axis})$ can be approximated as a constant A. Since we assume $\frac{v}{c} \ll 1$, we have $\beta_{i,j} \approx 1$ and thus this front term is approximately constant. We know at zero velocity this approximation should be equal to the exact expression for the noise correlation function over the given distribution of sound sources. Since $\rho(0,0) = 1$ for our virtual source, we have:

$$A = NCF(\tau^+, v_1 = 0, v_2 = 0) \tag{3.21}$$

Thus we can approximate the noise correlation function as:

$$NCF(\tau^+, v_1, v_2) \approx NCF(\tau^+, 0, 0)\rho(0, \dot{\mu}_{axis}) \tag{3.22}$$

which holds as long as our low velocity assumption is correct, and as demonstrated in Figure 3.2, this is reasonable for the AUEs.

The proposed approximation does two important things. First, it decouples

the effects of receiver velocity from the actual distribution of sound sources in our environment. Second, it shows the behavior of the noise correlation function at our time of interest looks like a scaled version of the behavior of a single source on the axis passing through the receivers.

3.5   Simulations

To confirm the proposed hypotheses on the noise correlation function's behavior under receiver velocity, we present simulation results. These results show our proposed virtual source model for the noise correlation function under receiver velocity holds well as a first order approximation.

3.5.1   Simulation Setup

Each simulation scenario begins with picking a distribution of sound sources and a set of paths for each receiver. We select the start and end position of each receiver for each velocity such that halfway through the correlation the receivers are the same distance apart. This ensures that we always have the same average separation over the correlation window regardless of the receiver velocity.

Sources are generated using independent bandpassed standard normal processes for a duration of 0.1 seconds. The spatial distribution of sources varies from experiment to experiment, however the distribution of start times is distributed uniformly over the experiment time window in all cases.

To propagate the sources to each receiver, we use the model in which the signal

received is given by:

$$s_{i,j}(t) = \left(\frac{1}{1+d}\right) s_j \left(\left(1 + \frac{v_{rel}}{c}\right)(t + D)\right) \tag{3.23}$$

which corresponds with our receiver having a constant velocity with respect to the source (reasonable since our sources are short in duration and our receivers move slowly) and attenuation due to spherical spreading $\approx \frac{1}{d}$ where d is the distance from source to receiver. The $\frac{1}{1+d}$ attenuation factor ensures that a source at 0 distance from our receiver experiences no attenuation and corresponds with a source origin power of $\sigma_s^2 = 1$.

Holding the source distribution constant, we generate audio as heard by each receiver for a set of constant velocities. We then repeat the experiment with a new realization of the source positions and start times for a set number of trials depending on the variance inherent in the distribution. For example, results from isotropic distributions tend to be noisier than those with sources only in the endfire beams, so we perform more trials on the isotropic distributions in order to increase the certainty of our results.

In simulation we explore the following source distributions:

1. Sources on the axis passing through the receiver pair

2. Sources distributed in the $2D$ endfire regions of the receiver pair

3. Sources distributed isotropically over the $2D$ plane containing the receivers

4. Receivers at constant $10m$ depth, sources distributed isotropically in a 2D plane at the surface

Case 1 serves as a verification of our intuition that sources on the axis behave like a single virtual source on each side of the receiver pair. Case 2 serves to demonstrate that our proposed approximation holds for sources in the endfire beams of the receivers. Cases 3 and 4 demonstrate the most realistic cases in which we test to see how well our approximation holds in isotropic sound field cases. Based on our previous discussion of noise from surface agitation, Case 4 is the most representative of a scenario we expect to see in practice.

After computing the empirical noise correlation function values for each value in each trial, we compute the mean and standard deviation of the estimates which we use to form 90% confidence intervals for the average noise correlation amplitude of each receiver pair velocity across our set of source distribution realizations. This gives us a relative sense of certainty about these empirical estimates.

These simulations are intended to demonstrate that our model does indeed reflect the behavior of the noise correlation function in a simple environment.

3.5.2   Simulation Results

First, we confirm our previous argument that the noise correlation function of a set of sources along the axis passing the receivers is well modeled by the ambiguity function of a single source on the axis.

Figure 3.6 demonstrates that as predicted, sources on the axis passing through our receiver pair can be modeled with a pair of virtual sources, one for each endfire beam of our receiver pair. Note that our peak value for the correlation is not equal to 0.5 for sources along the axis, due to the correlation pre-processing and sources between the two receivers contributing to peaks not at $\tau = \tau^+$ or $\tau = \tau^-$.
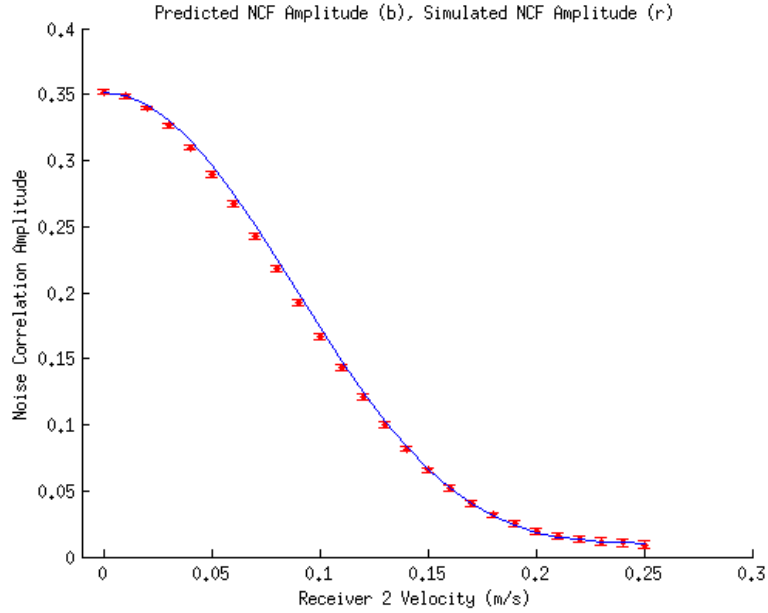
Figure 3.6: Predicted and simulated correlation coefficients for a single receiver moving, with all sources distributed uniformly along the axis between the two receivers. This confirms our intuition that many sources along the axis between the receivers behaves like a single source.

Next, we demonstrate that a field composed of only sources in the endfire beams is approximated by the ambiguity function for a single virtual source on the axis passing through the receivers.

Though not as good an approximation as the axis case, here we can see that our approximation holds reasonably well. In this case, the approximation tends to underbound the experimental bounds by a narrow margin. In the higher center frequency and bandwidth cases, the peak noise correlation value drops off much faster as a function of receiver velocity, but the approximation holds much more tightly because of the narrower endfire beamwidth in these cases.

In the cases with isotropically distributed noise, we start to see some interesting effects. Our approximation holds reasonably well for different bandwidths and center frequencies (Figures 3.8, and 3.9).
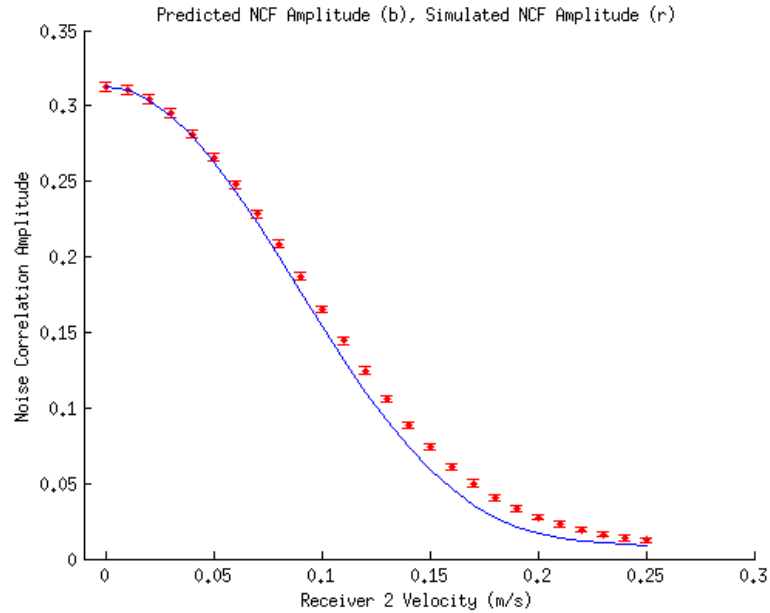
Figure 3.7: Simulated and predicted noise correlation amplitude for varying velocities with sources distributed in the endfire regions of the receivers. Blue line shows predicted values while red dots with 90% confidence intervals shows simulated results.

Finally, we get to the most realistic case of sources residing in a plane above the receivers, corresponding with surface noise above receivers at constant depth. Like the previous two cases, we see that our predicted noise correlation value tends to underbound the experimental data by a small margin. This is acceptable from a design perspective because it allows us to choose our correlation parameters such that we will achieve slightly better than predicted performance. Similar to the 2D case we see that our approximation works well in the surface noise case (Figures 3.10 and 3.11).
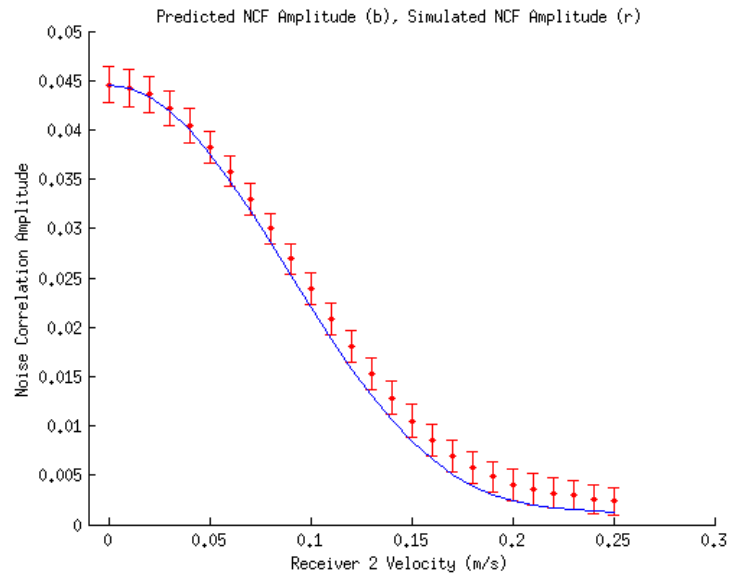
Figure 3.8: Simulated and predicted noise correlation amplitude for varying velocities with sources distributed isotropically in the $2D$ plane of the receivers, $B = 400$, $f_c = 300$. Blue line shows predicted values while red dots with 90% confidence intervals shows simulated results.
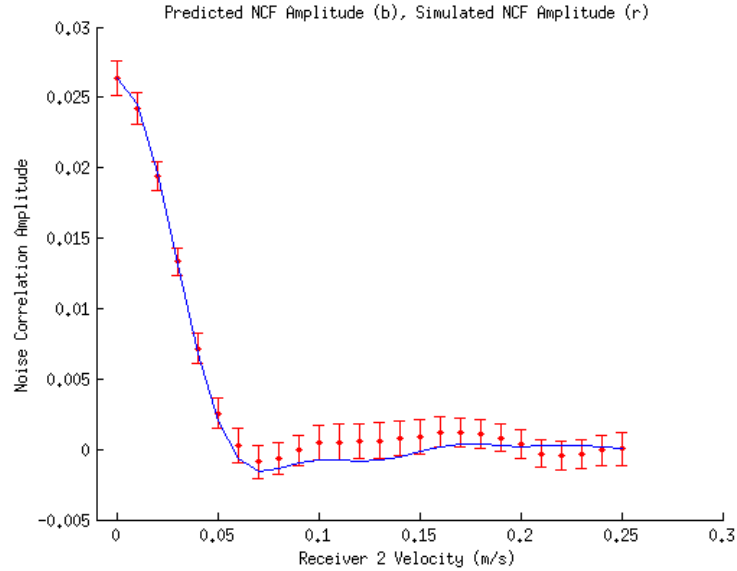

Figure 3.9: Simulated and predicted noise correlation amplitude for varying velocities with sources distributed isotropically in the $2D$ plane of the receivers, $B = f_c = 1000$. Blue line shows predicted values while red dots with 90% confidence intervals shows simulated results. We see here that increasing the center frequency makes the amplitude drop off faster with velocity.
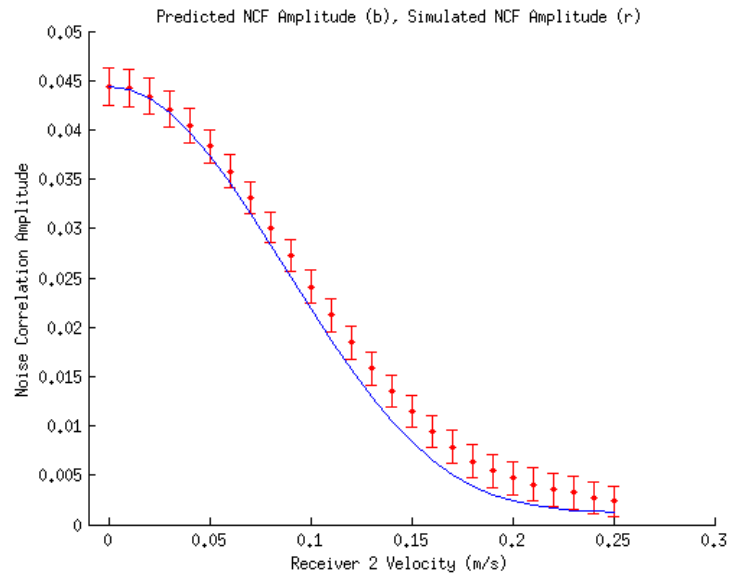
Figure 3.10: Simulated and predicted noise correlation amplitude for varying velocities with sources distributed isotropically on the surface plane 10m above the receivers, $B = 400$, $f_c = 300$. Blue line shows predicted values while red dots with 90% confidence intervals shows simulated results.
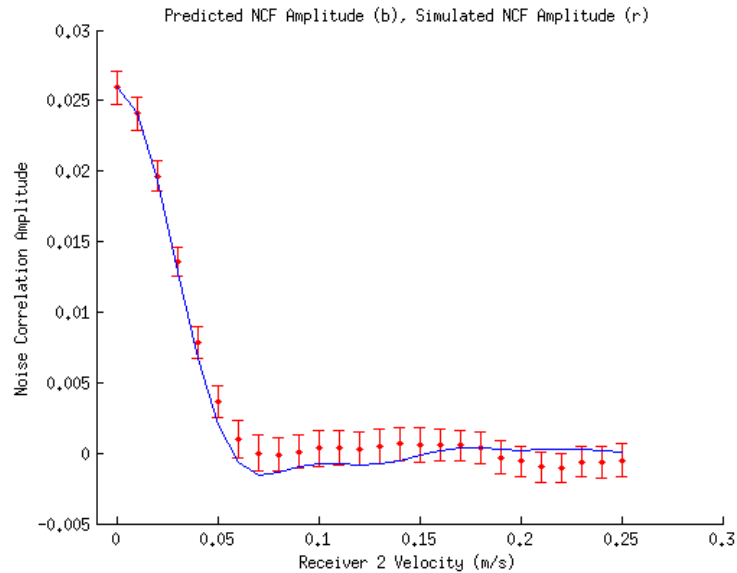

Figure 3.11: Simulated and predicted noise correlation amplitude for varying velocities with sources distributed isotropically on the surface plane 10m above the receivers with $B = f_c = 1000$. Blue line shows predicted values while red dots with 90% confidence intervals shows simulated results.

Chapter 4

Mobile Noise Correlation Function Design Space

This chapter explores the implications of our proposed mobile noise correlation function approximation on the choice of window length, bandwidth, and center frequency for computing the noise correlation function. From past literature we know that in the stationary case, longer correlation windows result in a higher SNR for our correlation peaks. However, from the results presented in Chapter 3, we know this is not the case when our receivers are mobile. To find the ideal correlation window, we apply past knowledge about the noise correlation SNR with our proposed approximation to estimate the optimal correlation time window for a given set of receiver velocities.

4.1   Noise Correlation SNR

As discussed in Chapter 2, we know the noise correlation function in the stationary case is proportional to:

$$SNR \propto \left(\frac{\sqrt{BT}}{\sqrt{f_c}} \right) \tag{4.1}$$

Applying the mobile case approximation from Equation 3.22 ($NCF(\tau^+, v_1, v_2) \approx NCF(\tau^+, 0, 0)\rho(0, \dot{\mu})$) in the mobile case to this SNR expression, we get:

$$SNR \propto \left(\frac{\sqrt{BT}}{\sqrt{f_c}} \right) \rho(0, \dot{\mu}) \tag{4.2}$$

$$\propto \left(\frac{\sqrt{BT}}{\sqrt{f_c}} \right) \frac{1}{BT\dot{\mu}} \left[Si \left(\pi\dot{\mu}T \left(f_c + \frac{B}{2} \right) \right) - Si \left(\pi\dot{\mu}T \left(f_c - \frac{B}{2} \right) \right) \right] \tag{4.3}$$

$$\propto \frac{1}{\sqrt{BT}f_c\dot{\mu}} \left[Si \left(\pi\dot{\mu}T \left(f_c + \frac{B}{2} \right) \right) - Si \left(\pi\dot{\mu}T \left(f_c - \frac{B}{2} \right) \right) \right] \tag{4.4}$$

This demonstrates that the noise correlation signal to noise ratio in the constant velocity case does not monotonically improve with increasing time windows. In terms of optimization, this provides us with an objective we can maximize over to get the best possible signal to noise ratio for given conditions. Also, noting that receiver velocity does not change the noise level in the region outside of the time-domain Green's function response, our signal amplitude drops with $\rho(0, \dot{\mu})$. Thus, given a minimum SNR we can use this to compute the maximum tolerable inter-node velocity such that we can recover a distance estimate between our receivers.

4.2   Time Window Selection

An interesting implication of this approximation is that we can use our knowledge of the single source ambiguity function to find the optimal correlation time window and bandwidth about a given center frequency in order to maximize our signal to noise ratio for a given receiver velocity. Most importantly, this illustrates the hypothesized ideal time window selection problem in which we want to pick a time window long enough for our correlation process to produce results but short enough for the receiver geometry to remain relatively constant. Figure 4.1 demonstrates this by showing the SNR objective surface over a set of possible bandwidth and time window values for different receiver velocities. We can see from this that as our velocity increases we must also decrease the time window to obtain the best results. Furthermore, as velocity increases, our sensitivity to the ideal time window increases as well.

As Figure 4.1 shows, we are almost always better off choosing larger bandwidth. Thus when choosing our correlation parameters in practice, we should choose the largest bandwidth which admits only the ambient sound sources we are interested in using.

4.3   Maximum Tolerable Velocity

Suppose we have a system in which we can successfully estimate distances between our receivers so long as the noise correlation function is a times its value in the stationary case for $a \in [0, 1]$. We can formulate the maximum tolerable inter-node

velocity problem then as:

$$\max_{v_{rel}}(v_{rel}) \tag{4.5}$$

$$\text{subject to:} \tag{4.6}$$

$$a \leq \rho\left(0, \frac{1 - \frac{v_{rel}}{2c}}{1 + \frac{v_{rel}}{2c}} - 1, f_c, B, T\right) \tag{4.7}$$

$$T \in [T_{min}, T_{max}] \tag{4.8}$$

$$f_c \in [f_{min}, f_{max}] \tag{4.9}$$

$$B \in [B_{min}, B_{max}] \tag{4.10}$$

$$\tag{4.11}$$

Given a range of parameter choices, this problem yields the maximum tolerable inter-node velocity for our system. Due to the non-convexity of constraint (4.7), this problem is difficult to solve directly. A strategy one could pursue instead would be to choose B and f_c based on environmental conditions, then performing a brute force optimization on Equation 4.5 since the condition (4.7) is reasonably easy to compute directly. After finding the maximum tolerable velocity, there may be many possible time windows which meet a certain level of performance. In general, one should use the largest time window possible which meets the velocity requirements of the system because it takes time for the noise correlation to converge to its expected value [6].

To find the maximum tolerable velocity for a given f_c and B we can trace the contour corresponding with our minimum performance requirement to its maximum velocity. As long as the corresponding time window is long enough for the noise statistics to converge well enough, we now have the tolerable velocity maximizing design. As mentioned before if more than one time window satisfies the design

requirements, we should choose the largest one so that the noise statistics have as much time as possible to converge. Figure 4.2 shows an example of a design space corresponding with $B = 400$, $f_c = 300$, with a noise statistics which take at least 15 seconds to converge. We can see that the maximum feasible velocity for a minimum $\rho(0, \dot{\mu}) = 0.8$ is around 0.12 m/s, which is achievable with a time window of 15 seconds. Figure 4.3 shows a design space with a higher center frequency of $f_c = 600Hz$ and bandwidth $B = 800Hz$ and we can see that since $\rho(0, \dot{\mu})$ drops off much faster with v, we have a much lower maximum tolerable velocity than the previous case.
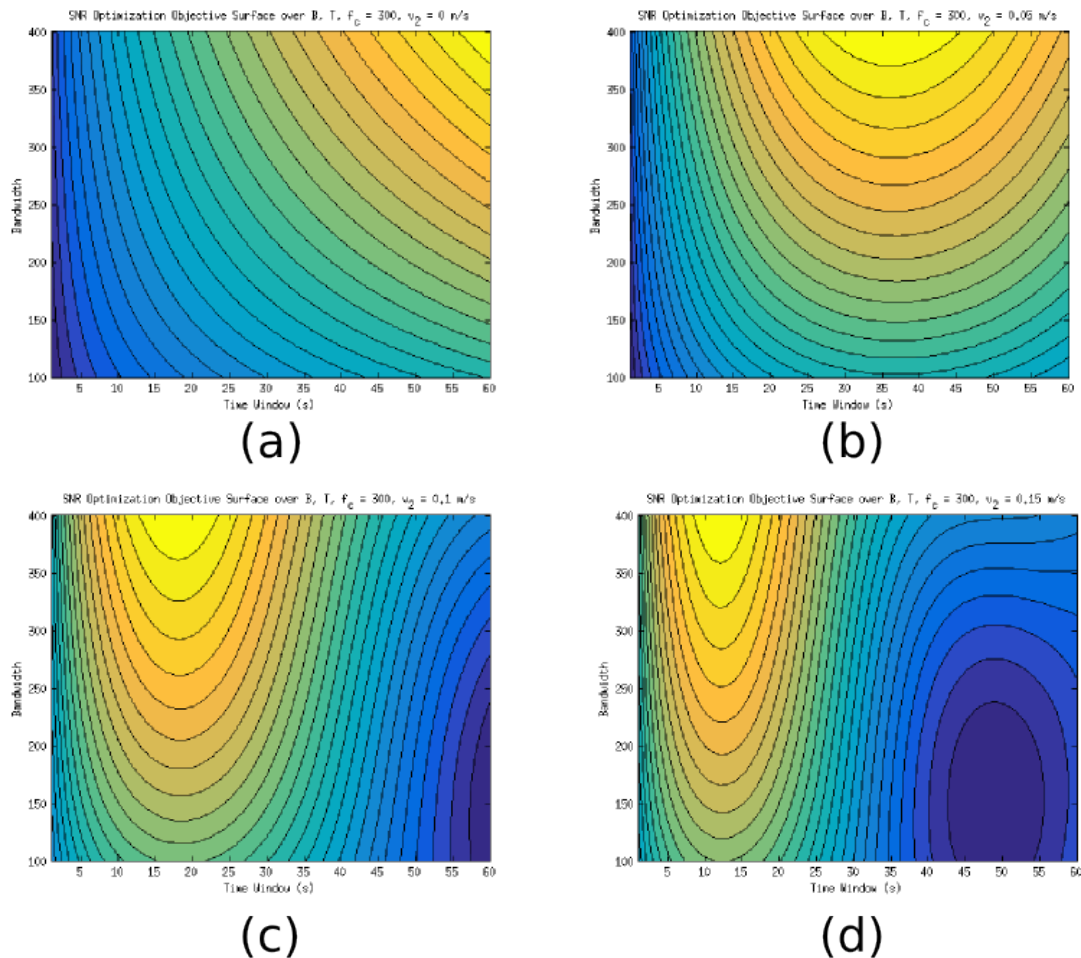
Figure 4.1: Design surfaces over correlation bandwidth and time, showing SNR objective for different fixed velocities. B is increasing on the y axis and T is increasing on the x axis, with $f_c = 300$. On the z axis, yellow (lighter) indicates a higher value for the SNR objective. (a): At 0 velocity, our best time and bandwidth are the maximum we can choose. (b): At $v = 0.05$ m/s the optimal time window is no longer the longest possible window. (c): Increasing the receiver velocity to $v = 0.1m/s$ our optimal time window is again smaller, however optimal bandwidth remains the largest we can choose. (d): At $v = 0.15m/s$ we can see that near optimal B, T, more bandwidth is better, however in the upper right of this plot (low B, high T) there are cases where increasing bandwidth does not improve the SNR at the given velocity.
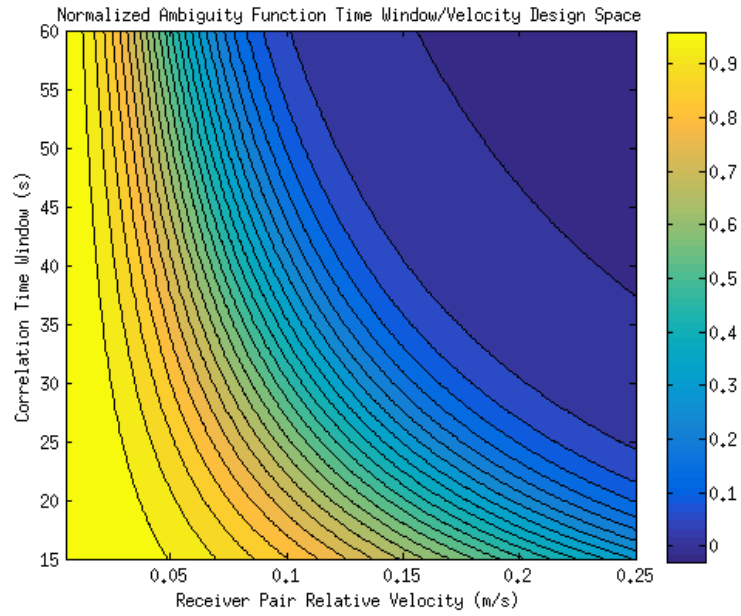
Figure 4.2: Maximum tolerable velocity design space for a center frequency of $300Hz$ and a bandwidth of $400Hz$. Z axis indicates $\rho(\gamma = 0, \dot{\mu})$ for the given receiver pair relative velocity and correlation time window.

Figure 4.3: Maximum tolerable velocity design space for a center frequency of $600Hz$ and a bandwidth of $800Hz$. Z axis indicates $\rho(\gamma = 0, \dot{\mu})$ for the given receiver pair relative velocity and correlation time window.
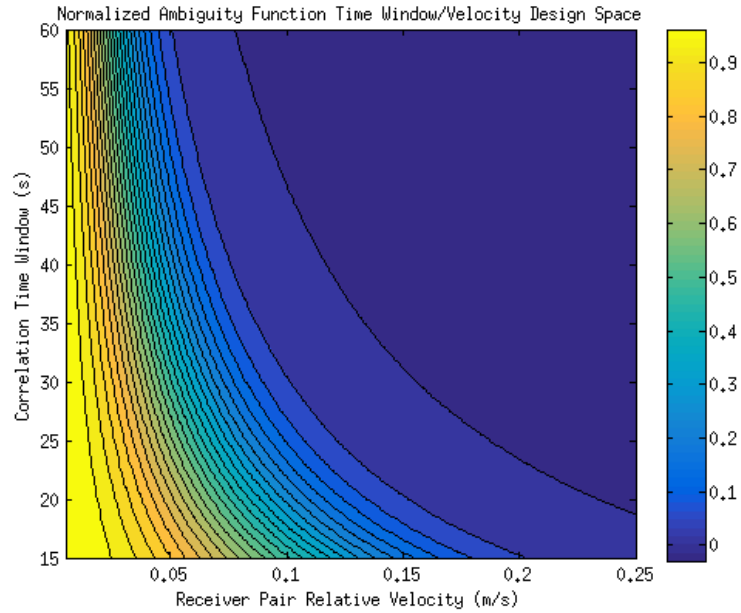
Chapter 5

Conclusion

In exploring the effects of receiver mobility on inter-node distance estimation via correlations of ambient noise we've demonstrated that we can model the mobile noise correlation problem using the wideband ambiguity function. By approximating the set of noise sources in the endfire beams of our receiver pair as a single virtual source, we can reduce the problem of finding the noise correlation function of a mobile receiver pair to solving the normalized wideband ambiguity function of a single source on the axis through the receivers. Through simulation on common sound source distributions we've shown that with appropriate scaling this approximation predicts the amplitude of the mobile noise correlation function reasonably well, typically underbounding the simulated values by a small margin. We then demonstrated how this approximation can be combined with past work on the SNR of the noise correlation function for a stationary set of receivers to choose correlation parameters like bandwidth and time window. We provided two examples of this, one showing the time and bandwidth parameters which maximize the SNR for a given receiver velocity and center frequency, and one showing the maximum tolerable velocity and the largest time window which

achieves the required performance.

As stated in the acknowledgements I'd like to thank my advisors Ryan Kastner and Curt Schurgers, and lab partner Perry Naughton for their mentorship, collaboration, and assistance in submitting elements of this work as a conference paper to IEEE OCEANS 2016.

Bibliography

[1] J. Jaffe and C. Schurgers, "Sensor networks of freely drifting autonomous underwater explorers," in *Proceedings of the 1st ACM international workshop on Underwater networks*, pp. 93–96, ACM, 2006.

[2] J. S. Jaffe, R. Glatts, C. Schurgers, D. Mirza, P. J. Franks, P. Roberts, and F. Simonet, "Aue: An autonomous float for monitoring the upper water column," in *OCEANS 2007-Europe*, pp. 1–4, IEEE, 2007.

[3] D. Mirza, P. Roberts, J. Yi, C. Schurgers, R. Kastner, and J. Jaffe, "Energy efficient signaling strategies for tracking mobile underwater vehicles," in *Underwater Technology Symposium (UT), 2013 IEEE International*, pp. 1–8, IEEE, 2013.

[4] X. Ji and H. Zha, "Sensor positioning in wireless ad-hoc sensor networks using multidimensional scaling," in *INFOCOM 2004. Twenty-third AnnualJoint Conference of the IEEE Computer and Communications Societies*, vol. 4, pp. 2652–2661, IEEE, 2004.

[5] P. Roux and M. Fink, "Greens function estimation using secondary sources in a shallow water environment," *The Journal of the Acoustical Society of America*, vol. 113, no. 3, pp. 1406–1416, 2003.

[6] K. G. Sabra, P. Roux, and W. A. Kuperman, "Emergence rate of the time-domain greens function from the ambient noise cross-correlation function," *The Journal of the Acoustical Society of America*, vol. 118, no. 6, pp. 3524–3531, 2005.

[7] G. M. Wenz, "Acoustic ambient noise in the ocean: spectra and sources," *The Journal of the Acoustical Society of America*, vol. 34, no. 12, pp. 1936–1956, 1962.

[8] P. Roux, W. Kuperman, N. Group, *et al.*, "Extracting coherent wave fronts from acoustic ambient noise in the ocean," *The Journal of the Acoustical Society of America*, vol. 116, no. 4, pp. 1995–2003, 2004.

[9] K. G. Sabra, P. Roux, A. M. Thode, G. L. D'Spain, W. Hodgkiss, and W. Kuperman, "Using ocean ambient noise for array self-localization and self-synchronization," *Oceanic Engineering, IEEE Journal of*, vol. 30, no. 2, pp. 338–347, 2005.

[10] E. Kelly and R. Wishner, "Matched-filter theory for high-velocity, accelerating targets," *Military Electronics, IEEE Transactions on*, vol. 9, no. 1, pp. 56–69, 1965.

[11] P. M. Woodward, *Probability and Information Theory, with Applications to Radar: International Series of Monographs on Electronics and Instrumentation*, vol. 3. Elsevier, 2014.

[12] G. Johnson, D. Ohlms, and H. Hampton, "Broadband correlation processing," in *Acoustics, Speech, and Signal Processing, IEEE International Conference on ICASSP'83.*, vol. 8, pp. 583–586, IEEE, 1983.